Flexible and Printed Electronics

ACCEPTED MANUSCRIPT

Low-profile flexible frequency-reconfigurable millimetre-wave antenna for 5G applications

To cite this article before publication: Syeda Fizzah Jilani *et al* 2018 *Flex. Print. Electron.* in press https://doi.org/10.1088/2058-8585/aad392

Manuscript version: Accepted Manuscript

Accepted Manuscript is "the version of the article accepted for publication including all changes made as a result of the peer review process, and which may also include the addition to the article by IOP Publishing of a header, an article ID, a cover sheet and/or an 'Accepted Manuscript' watermark, but excluding any other editing, typesetting or other changes made by IOP Publishing and/or its licensors"

This Accepted Manuscript is **© 2018 IOP Publishing Ltd**.

During the embargo period (the 12 month period from the publication of the Version of Record of this article), the Accepted Manuscript is fully protected by copyright and cannot be reused or reposted elsewhere.
As the Version of Record of this article is going to be / has been published on a subscription basis, this Accepted Manuscript is available for reuse under a CC BY-NC-ND 3.0 licence after the 12 month embargo period.

After the embargo period, everyone is permitted to use copy and redistribute this article for non-commercial purposes only, provided that they adhere to all the terms of the licence https://creativecommons.org/licences/by-nc-nd/3.0

Although reasonable endeavours have been taken to obtain all necessary permissions from third parties to include their copyrighted content within this article, their full citation and copyright line may not be present in this Accepted Manuscript version. Before using any content from this article, please refer to the Version of Record on IOPscience once published for full citation and copyright details, as permissions will likely be required. All third party content is fully copyright protected, unless specifically stated otherwise in the figure caption in the Version of Record.

View the article online for updates and enhancements.

This content was downloaded from IP address 142.132.1.147 on 19/07/2018 at 17:30

IOP Publishing Journal Title
Journal **XX** (XXXX) XXXXXX https://doi.org/XXXX/XXXX

Low-profile flexible frequency-reconfigurable millimetre-wave antenna for 5G applications

Syeda Fizzah Jilani[1], Ardavan Rahimian[1], Yasir Alfadhl[1], and Akram Alomainy[1]

[1] School of Electronic Engineering and Computer Science, Queen Mary University of London, London E1 4NS, U.K.

E-mail: s.f.jilani@qmul.ac.uk

Received xxxxxx
Accepted for publication xxxxxx
Published xxxxxx

Abstract

This paper presents the design and characterisation of a flexible, inkjet-printed, low-profile, and frequency-reconfigurable antenna, intended for the fifth generation (5G) wireless networks operating at millimetre-wave (mm-wave) frequency bands. The antenna geometry is comprised of a slotted T-shaped radiating patch embedded in a rectangular aperture cut inside the ground plane. The slots are designed with two pairs of switches to reconfigure the radiating area for the desired selection of operating frequency at the K_a-band (26.5–40 GHz). Moreover, a two-element inkjet-printed multiple-input multiple-output (MIMO) antenna assembly is proposed based on a flexible polyethylene terephthalate (PET) film. The conformal MIMO antenna is suitable for integration in high-performance flexible 5G front-ends, as well as in next-generation wearable electronic devices and applications.

Keywords: 5G, flexible, MIMO antenna, reconfigurable, wireless

1. Introduction

Flexible and conformal electronic devices and antennas are anticipated as essential features of 5G architecture, in order to maximise the feasibility of integrating the wireless technology in numerous smart applications for the compact, robust, and reliable user experience [1]. The vision of 5G is not limited to handheld cellular devices, and is expected to deliver a versatile and diverse network, in which device miniaturisation, flexible implements, lightweight, and cost-effectiveness are the key considerations. Recent progress in the development of fast, precise, and low-cost manufacturing techniques on flexible substrates, such as the inkjet printing, screen printing, or laser prototyping, has made possible numerous wearable wireless applications integrated with flexible and conformal antennas and circuits [2, 3]. However, most of the flexible antennas are reported for the low-frequency operation and more profound efforts are needed for the design and potential implementation of high-frequency flexible antennas for 5G.

Future wireless networks are anticipated to deliver high data rates and extended capacity by enabling deployment of small cells in a dense environment. The mm-wave spectrum has attracted a huge research interest in progressing toward an ultra-fast infrastructure, in order to facilitate an increasing user demands, as well as the drastic advancement of services and applications for 5G systems [4–6]. Suitability of K_a-band is emphasised for 5G cellular networks in a number of platforms among the unused high-frequency bands due to the lower atmospheric attenuations, reduced propagation losses, and relatively lesser degradation of the signal strength caused by shadowing and multipath fading within a picocell [7–9]. The realisation of 5G mm-wave architectures has necessitated the deployment of efficient, adaptable, and flexible antennas at the wireless front-ends. Frequency-reconfigurable antennas have a substantial contribution in recent cognitive radio systems, due to adaptable operation at distinct bands, as well as the capability to alter the physical geometry which can shift the resonance toward the intended frequency [10]. This feature is highly influential in 5G to enhance the data throughput due to an increase in the bandwidth and capacity [11, 12].

Accepted Manuscript

 © xxxx IOP Publishing Ltd

The surface-mount switching schemes such as PIN diodes [13], FETs [14], MEMS [15], and varactors [16] with suitable characteristics of insertion loss, isolation, linearity, size, and cost are usually employed within antenna geometry to perform reconfiguration. In this work, the reconfiguration validation is carried out by ideal switches (i.e., open/short metal contacts) to avoid complexity; however, surface-mount switches will be used in future for the practical implementation. MIMO arrays combine a number of antenna elements acting as independent channels to support simultaneous data throughput. After the deployment in the 4G and LTE networks, MIMO antennas are regarded as a promising technology for 5G networks [17]. Integration of the frequency-reconfigurable MIMO antennas is crucial for efficient spectrum utilisation, since it delivers a control over the frequency selection and capacity [18].

This work presents the aggregation of both the MIMO and frequency-reconfiguration schemes on a flexible and bendable antenna, in order to develop compatibility with 5G wearable applications. Flexible antennas have been implemented on versatile materials, such as textile, polymers, polyimides, and polyesters [19]. Ultra-thin and conformal films, such as PET and Kapton, are among the feasible substrates for the printed antennas, due to suitable material properties and low-cost [20, 21]. The additive manufacturing technique of inkjet printing is effectively used for accurate fabrication of several printed circuits and antennas [22, 23]. For instance, the inkjet printing process by using silver nanoparticle ink has been deployed on a flexible polydimethylsiloxane (PDMS) substrate in [24] and on PET substrate in [25] for a wearable antenna fabrication. Also, carbon-based compounds such as graphene and carbon nanotubes (CNTs) are gaining huge attention in the printable and flexible electronics to replace conductive metal inks. A flexible and stretchable antenna is proposed on a stretchable single-walled carbon nanotubes (SWCNTs)/Lycra fabric [26]. Moreover, the stretchable conductive ink solutions compatible with the body-centric wearable antennas are presented [27]. In this work, a flexible and frequency-reconfigurable PET-based MIMO antenna has been developed, and the performance has been evaluated for the potential deployment in 5G networks.

2. Antenna design and fabrication

In this section, the antenna design and modelling, as well as the fabrication of the antenna using inkjet printing process are addressed. Also, the material characterisation in terms of the profilometer measurements of PET surface and imaging using scanning electron microscope (SEM) is provided.

2.1 Antenna design and modelling

The antenna design integrates frequency reconfiguration and MIMO configuration on a flexible substrate which adds an advantage of antenna placement even on irregular surfaces. The CST STUDIO SUITE has been used for the analytical design and numerical modelling, which has been conducted based on the finite integration technique (FIT) using the robust transient solver to evaluate the time-domain characteristics of the antenna structure. The design process is initiated with a single antenna element, comprised of a slotted T-shaped patch and a coplanar waveguide (CPW) feeding. This type of slotted patch geometry enables a compact and small footprint along with the incorporated switches for the reconfiguration [28]. The ground plane is designed with an etched-off rectangular aperture for the placement of the antenna.

Integration of a pair of symmetrical slots terminated with *x*-pair of switches is carried out on the patch to reconfigure the frequency based on the state of the switches. The flexible antenna resonates at 28-GHz when both the switches are OFF, as the slot-edges act as an open-circuit. While the resonant frequency band shifts to 38-GHz when both switches are ON, the radiating length is trimmed off as the slot-edges act as a short circuit. Furthermore, the design is modified with another pair of symmetrical slots provided with *y*-pair of switches which results in two additional operating modes. In order to diversify the flexible antenna functionality as a standalone transmitter and a receiver, a two-element MIMO assembly is introduced for the designed antenna configuration. Fig. 1 (a) shows the proposed MIMO antenna, and the dimensions of the design parameters are given in Table 1. Moreover, DC-biasing is required to change the switch-state, while implementing the actual switches, e.g., PIN diodes. Here, if the *x*-/*y*-switch is applied with a potential difference, the metal short parallel to the switch, denoted by *z* in Fig. 1 (a), would provide a path for the DC current, and the switch would not be enabled. Hence, a gap of 0.1 mm is inserted at *z*, along with a 0.1 μF capacitor, which blocks the DC from *z* without interrupting the AC flow and the DC current is directed through the switch.

Table 1. Dimensions of the inkjet-printed 5G MIMO antenna.

Symbol	Parameters	(mm)
L_p	Length of patch	5.7
W_p	Width of patch	2.05
L_s	Length of ground slot	5.3
W_s	Width of ground slot	6.1
L	Length of MIMO antenna	11
W	Width of MIMO antenna	25.4
a	Distance of slot-1 from the feed	1.05
b	Distance of slot-2 from the feed	1.8
L_f	Length of CPW ground	4.7
w	Distance of ground slot from CPW	2.15

2.2 Antenna fabrication and characterisation

The designed MIMO antenna is fabricated on the surface-treated PET film, with the thickness (h) = 135 ± 12 μm, dielectric constant (ε_r) = 3.2, loss tangent (tanδ) = 0.002, and dimensions of 11 × 25.4 mm^2 from the Mitsubishi Paper Mills Ltd., as shown in Figs. 1 (b) and (c). Moreover, the in-house

Accepted Manuscript

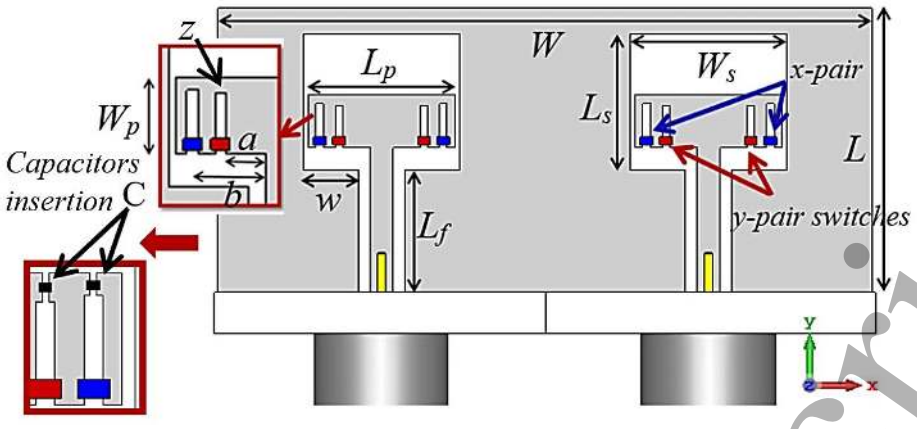

(a)

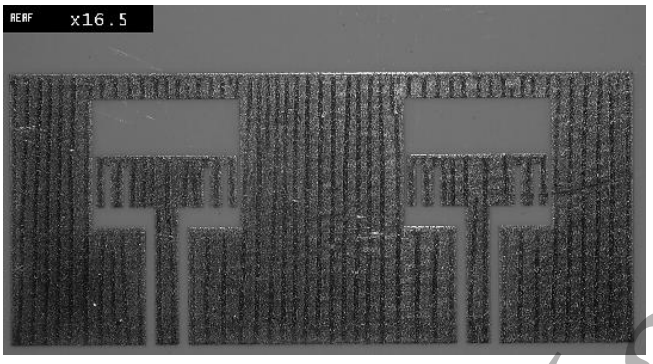

(b)

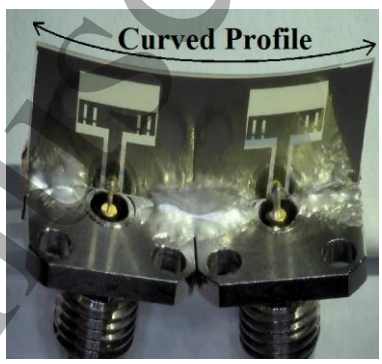

(c)

Fig. 1. Proposed flexible mm-wave frequency-reconfigurable two-element MIMO antenna: (a) simulated antenna model; (b) inkjet-printed fabricated antenna prototype; (c) realised conformal two-element MIMO antenna.

Dimatix materials printer (DMP-2831) is used for the antenna prototyping, along with the silver nanoparticle ink (i.e., Colloidal Ag-J solid Ag from Printed Electronics Ltd). The silver nanoparticles are encapsulated with the organic polymer coating to avoid the oxidation, and are dispersed in an inert solvent. The selected ink comprises of 20.3% of solid silver content by weight, suspended in a solution of water (40–50%), glycerol (30–40%), and acetylene glycol (0.1–1.0%). The conductive ink has a viscosity of 4.2 mPa.s, the surface tension of 30.5 mN/m, and density of 1.22 g/cm^3. The post-printing processes of drying, curing, and sintering are essential to release the particles from the polymer sheath and combine them into a firm conductive layer.

The conductivity of the printed layer is 0.4 ~ 2.5 × 10^7 S/m, and depends on the number of successive printing iterations, layer thickness, temperature, and time durations involved in both the curing and sintering processes. It is worth noting that an accurate and careful sintering results in the conductivity of 0.3 ~ 0.7 × 10^7 S/m from one printing iteration. To accomplish the fabrication, the printer has been appropriately calibrated in terms of the drop spacing, jetting frequency, waveform, printhead temperature, and firing voltage of the ejecting nozzles. The drop-spacing of 15 μm (i.e., 1693.33 dpi), firing voltage of 15 V, and jetting frequency of 5-KHz have been set in this regard. The variation in the surface profile of PET is characterised by using a profilometer, as in Fig. 2 (a), and utilised while adjusting the printhead position. A conductive layer with a thickness of 0.5 μm is deposited on a PET film with a pattern resolution of ±20 μm.

The PET substrates are provided with a chemically active microporous adhesive coating to enable the rapid drying and chemical sintering of the ink. This chemical method avoids laser exposure or high-temperature treatments that may result in the bending, shrinking, decolourisation, or melting, if the temperature is not appropriately handled. The microporous coating elevates the surface energy of the PET and improves the adhesion by chemically bonding the ink with the surface molecules, and restricts the ink flow outside the boundaries of a definite pattern for a precise prototyping. Another advantage of the chemical coating is to replace the actual surface of PET with a microporous surface, which allows partial diffusion of silver nanoparticles to facilitate better locking between the ink particles and surface molecules that results in a high adhesion and prevents the layer from peeling off.

The conformal assembly of antenna involves bending of the prototype, which may cause cracking of the layer with time.

Accepted Manuscript

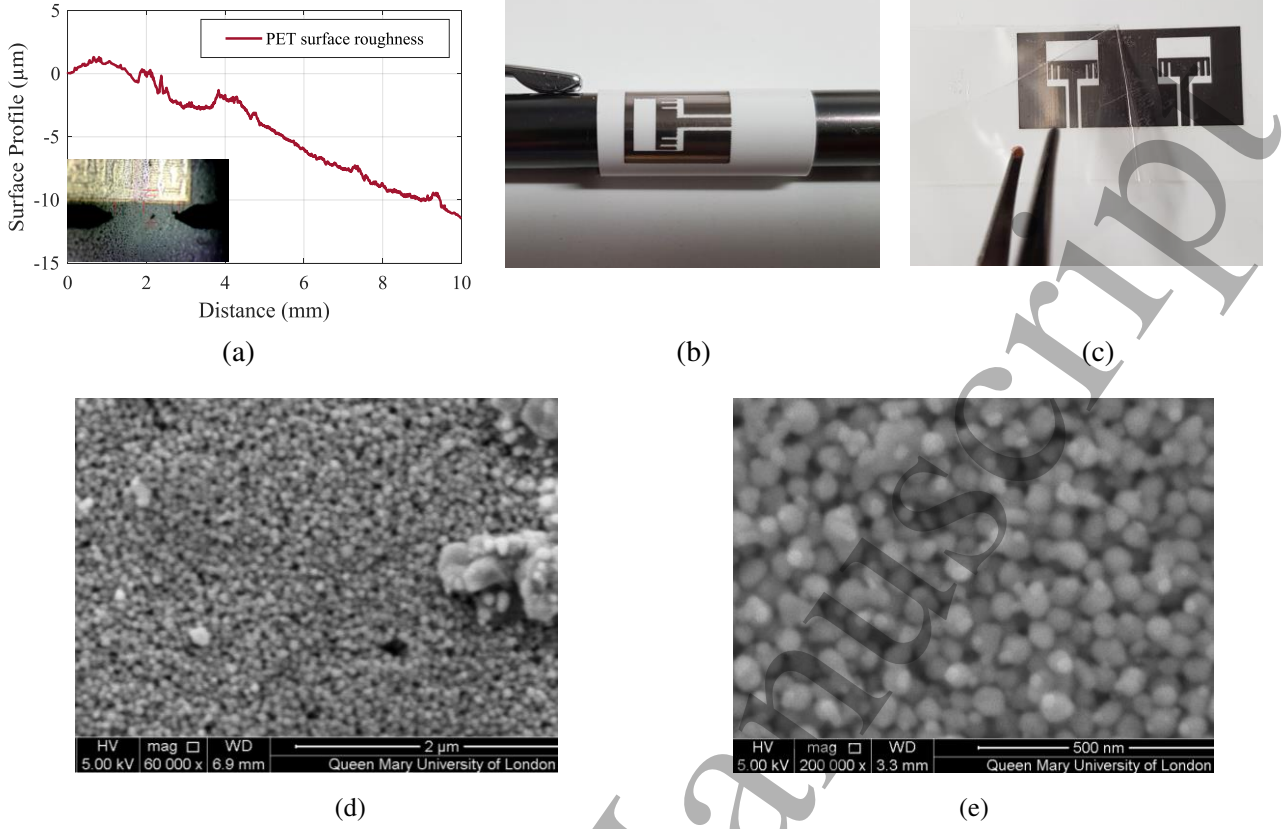

Fig. 2. Post-printing characterisation of the inkjet-printed antenna prototype, (a) surface profile of PET substrate by profilometer measurements; (b) conformal mount on a cylindrical surface of diameter 0.8 mm for the crack analysis; (c) adhesion testing by the scotch tape; (d) SEM image of the nanoparticle ink at 4 μm resolution; (e) SEM image of nanoparticle ink at 500 nm resolution.

In this regard, the thickness of the printed layer is critical, as thicker metal layers are more brittle and can be easily cracked by successive bending and folding. For instance, the screen printed layer is usually 10–20 μm thick with relatively larger particle size, which makes it less flexible and more prone to cracks than the inkjet-printed nanoparticle layer (i.e., 0.5 μm thick). The antenna is firmly mounted on a cylindrical surface of a 0.8 mm-diameter pen along the axial, circumferential, and diagonal axes, as in Fig. 2 (b). The post-bending microscopic inspection depicts no cracks. In addition, the standard scotch-tape test is performed to examine the robustness [29, 30]. The tape is glued to the printed pattern and then peeled off while the printed trace remains fully intact on the substrate, as in Fig. 2 (c), and exhibits the excellent ink adhesion and robustness. The prototype is also found water-resistant when submerged in water. Moreover, to obtain a clear insight, SEM imaging of the printed silver pattern is performed that shows the granular nature of the ink layer, as depicted in Figs. 2 (d) and (e).

3. Numerical and experimental analysis

Four switch configurations are realised by constructing the electrically-short/-open paths, where the short shows the ON mode, and the open one depicts the OFF mode, as in Figs. 3 (a) to (d). The antenna performance is analysed in a parametric study, and validated by experimental testing of the prototype. The analysis of scattering (S)-parameters, radiation pattern, and gain shows that measurements are in a good agreement with simulations, though some mismatches exist due to the fabrication intolerances, and connector and cable losses.

3.1 Impedance bandwidth

In order to inspect the antenna response toward conformity by the experimental testing and measurements, the fabricated MIMO antenna is mounted on K-connectors in both planar and conformal assemblies (curved surface of 3 cm-radius). Fig. 3 presents the measured results of the reflection coefficient (i.e., S_{11}/S_{22}) plots of the developed planar and conformal MIMO antenna for the proposed switch configurations, represented by the corresponding unit-cell and also shown in Table 2. The overall bandwidth of 27.3–40 GHz has been covered in the four switching modes of the reconfigurable MIMO antenna.

The measured transmission coefficients in the operating modes are depicted in Fig. 4 that shows lower mutual coupling and high isolation between the two adjacent antennas mounted

Accepted Manuscript

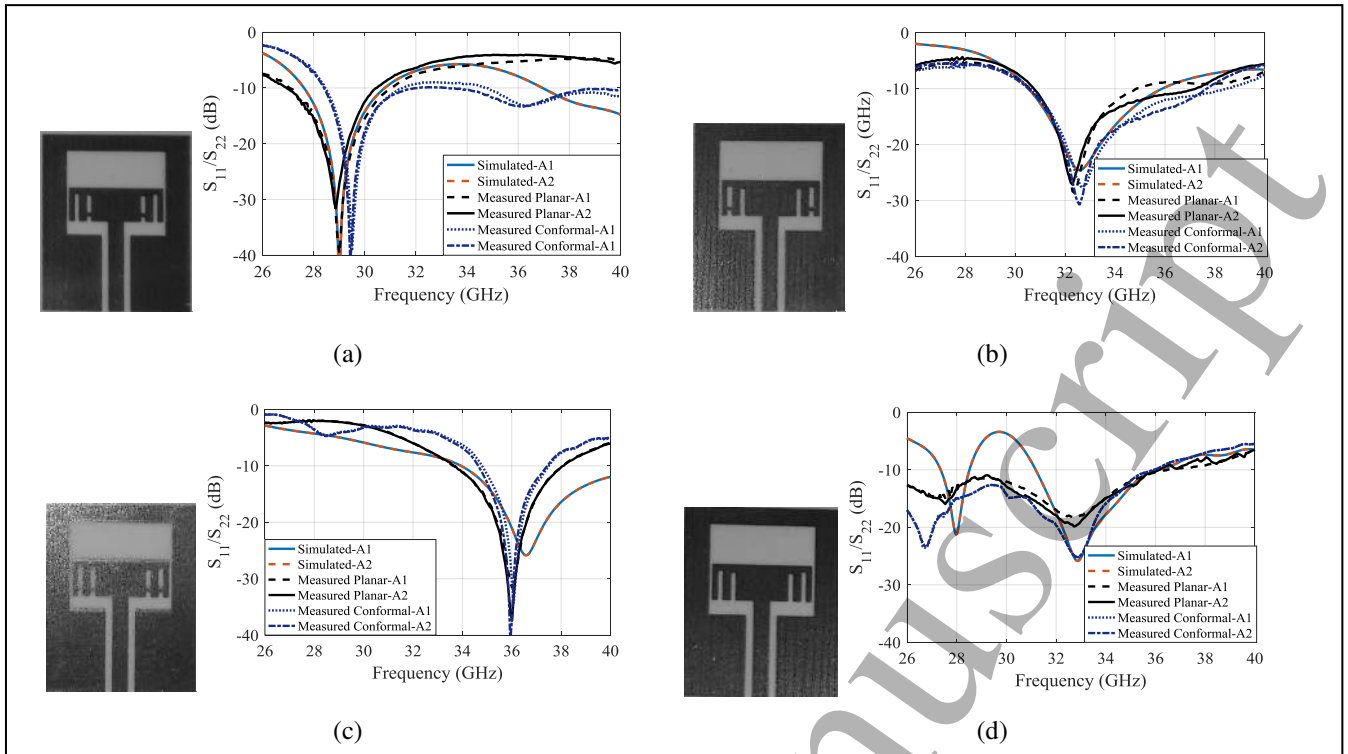

Fig. 3. Simulated and measured S_{11}/S_{22} plots of the flexible mm-wave frequency-reconfigurable two-element (i.e., A1 and A2) MIMO antenna, along with the unit-cell representation: (a) mode-I; (b) mode-II; (c) mode-III; (d) mode-IV.

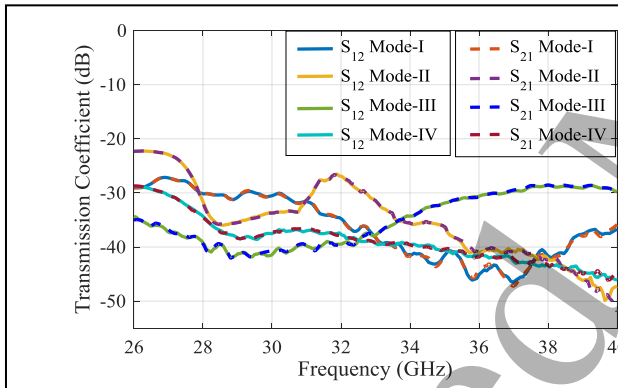

Fig. 4. Measured transmission coefficients (S_{12}/S_{21}) of the flexible mm-wave frequency-reconfigurable two-element MIMO antenna for four distinct modes.

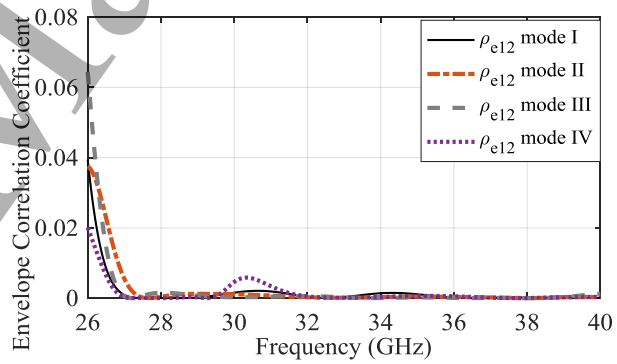

Fig. 5. Simulated envelope correlation coefficient plots of the flexible mm-wave frequency-reconfigurable two-element MIMO antenna.

in a planar assembly. The standard distance between adjacent elements in an array should be in-between $\lambda/2$ to λ, to avoid mutual coupling, i.e., higher the distance lower the coupling; however, increasing the distance might result in grating lobes [31, 32]. The proposed antenna is a T-shaped patch with more width than a rectangular patch or $\lambda/2$, which suggests more spacing between the patches' centres. The optimal level of the isolation suggests the transmission coefficients of at least –10 dB or below. It has been observed in the parametric study for achieving a high isolation, the optimal distance between the centres should be approximately 11 mm (i.e., equals to λ at 27.2-GHz that is the lower cut-off frequency). However, the distance between the centres is slightly increased due to larger patch width and is set at 12.7 mm in this proposed MIMO antenna, to accomplish a high isolation below –20 dB. The envelope correlation coefficient (ρ_e) is computed to evaluate the independence of the antenna elements for their individual operation in a MIMO assembly, and calculated based on the *S*-parameters. In this regard, Fig. 5 presents the low values of the numerically estimated ρ_e of the MIMO antenna, which depicts insignificant influence of neighbouring element on the performance of the single antenna.

Accepted Manuscript

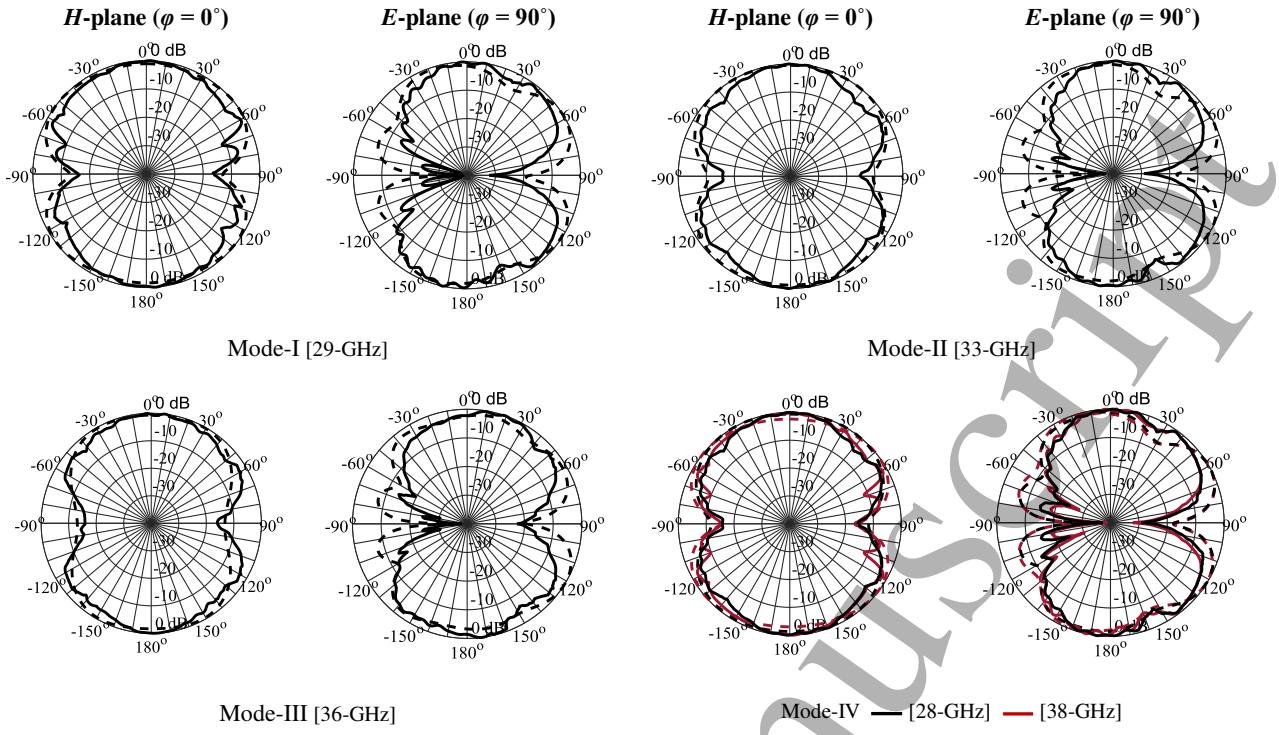

Fig. 6. Simulated and measured normalised far-field radiation patterns of the flexible mm-wave frequency-reconfigurable single antenna (i.e., unit-cell) of the MIMO configuration.

Table 2. Switch configurations of the 5G MIMO antenna.

Mode	SW-*x*	SW-*y*	Band	Bandwidth
Mode-I	OFF	ON	28-GHz	27.4–30.1 GHz
Mode-II	ON	OFF	33-GHz	30.5–35.9 GHz
Mode-III	ON	ON	37–39 GHz	34–40 GHz
Mode-IV	OFF	OFF	Dual-Band	27.3–28.5 GHz 31.1–36 GHz

3.2 Radiation pattern

The radiation characteristics of the developed antenna are measured by using the NSI near-field scanning setup for K_a-band that exhibits a precise near-field to far-field algorithm to compute the far-field radiation patterns. An evenly distributed pattern on the front and bottom with the maximum directivity perpendicular to the surface of the antenna has been observed throughout the operating range. Fig. 6 presents the simulated and measured results of a single element (i.e., a unit cell of the MIMO) at φ = 0˚ and φ = 90˚ at distinct frequencies of the operating modes I–IV. As the patch antenna is placed in the aperture cut inside the ground, it causes the surrounding metallic ground to act as a loop or frame, which confines the radiation of the patch orthogonal to the antenna plane (i.e., along the front and back directions), while the radiation is partially trimmed off along the antenna plane, as shown by the two orthogonal cuts (i.e., *E*- and *H*-planes) of the Fig. 6.

3.3 Realised gain

In a MIMO antenna, each element operates individually, hence, the peak gain of a single antenna is more important to be determined rather than the gain profile of a collective array. The simulated and measured results of the realised peak gain for a single antenna (i.e., unit-cell) of the proposed MIMO configuration over the operating range of 28–40 GHz have been tabulated in Table 3 for the operating modes I–IV. The gain is computed based on the measurements carried out in the near-field scanning, and the Two-Antenna Gain method is also utilised for the calculations. The measured gain shows similar findings as obtained by the simulated evaluations.

Table 3. Realised gain (dBi) vs. frequency for the switch configurations of the single antenna (i.e., unit-cell).

Freqency (GHz)		**28**	**30**	**32**	**34**	**36**	**38**	**40**
Mode-I	Simulated	2.7	3.8	–	–	–	–	–
	Measured	2.5	3.4	–	–	–	–	–
Mode-II	Simulated	–	–	4.6	3.7	–	–	–
	Measured	–	–	4.4	3.4	–	–	–
Mode-III	Simulated	–	–	–	6.5	4.7	4.2	4.4
	Measured	–	–	–	6.2	4.6	4.1	4.2
Mode-IV	Simulated	2.7	–	4.3	3.7	5.24	–	–
	Measured	2.5	–	4.2	3.5	4.9	–	–

Accepted Manuscript

The proposed MIMO antenna, which depicts the advantage of combining the flexibility, reconfiguration mechanism, and MIMO technology within a single antenna prototype has been compared with the recent progress of 5G antenna designs in Table 4. Several flexible and wearable antennas are reported for 5G, and significant work is also conducted at the mm-wave bands to develop MIMO antennas for 5G along with adaptable antennas for the frequency selection. In this regard, this work has undertaken the aggregation of these advanced wireless technologies, in order to deploy a novel and efficient antenna solution for the next-generation communication systems.

Table 4. Comparison of the proposed antenna with the recent 5G antennas.

Ref.	Size (mm^2)	Flex.	5G Bands (GHz)	Recon.	MIMO
[33]	23.5×36	×	26.8–28.4	×	✓ 2×4
[12]	16×14	✓	20.7–36	✓	×
[34]	12×50.8	×	25.1–37.5	×	✓ 1×4
[35]	14×10.5	✓	55–64.8	×	×
[36]	70×40	×	2.4, 27–29	×	✓ 4×4
Prop.	11×25.4	✓	27.3–40	✓	✓ 1×2

4. Conclusion

This paper has presented a novel flexible MIMO antenna at the mm-wave bands for the potential employment in the 5G wireless networks. The developed inkjet-printed PET-based antenna has provided a low-profile, lightweight, compact, and conformal two-element MIMO assembly with the suitability of integration on both the planar and non-planar surfaces. The antenna patch is incorporated with the two pairs of slots and switches and is capable of frequency reconfiguration in K_a-band. Experimental validation has been conducted by using open/short metallic switches, while surface-mount switches could be employed. The antenna covers an overall bandwidth of 27.3–40 GHz in the four distinct modes with a measured peak gain of 6.2 dBi at 34-GHz. In addition, the conformal MIMO antenna is able to provide the frequency selection, and the multi-channel transmissions, by combining the advanced technologies of MIMO and frequency-reconfiguration.

References

[1] Elobaid H A E *et al* 2017 A transparent and flexible polymer-fabric tissue UWB antenna for future wireless networks *IEEE Antennas Wireless Propag. Lett.* **16** 1333–1336

[2] Godlinski D *et al* 2017 Printing technologies for the manufacturing of passive microwave components: antennas *IET Microwav. Antennas Propag.* **11** 14 2010–2015

[3] Chen M Y *et al* 2012 Conformal ink-jet printed C-band phased-array antenna incorporating carbon nanotube field-effect transistor based reconfigurable true-time delay lines *IEEE Trans. Microwave Theory Tech.* **60** 1 179–184

[4] Rappaport T *et al* 2013 Millimeter-wave mobile communications for 5G cellular: it will work! *IEEE Access*, **1**, 335–349

[5] Pi Z and Khan F 2011 An introduction to millimeter-wave mobile broadband systems *IEEE Commun. Mag.* **49** 6 101–107

[6] Rahimian A *et al* 2016 Analytical and numerical evaluations of flexible V-band Rotman lens beamforming network performance for conformal wireless subsystems *Progress In Electromagn. Research B* **71** 77–89

[7] Hong W, Baek K H, and Ko S 2017 Millimeter-wave 5G antennas for smartphones: overview and experimental demonstration *IEEE Trans. Antennas Propag.* **65** 12 6250–6261

[8] Wang C X *et al* 2014 Cellular architecture and key technologies for 5G wireless communication networks *IEEE Commun. Mag.* **52** 2 122–130

[9] Rangan S, Rappaport T S, and Erkip E 2014 Millimeter-wave cellular wireless networks: potentials and challenges *Proc. IEEE*, **102** 3 366–385

[10] Mansoul A *et al* 2014 A selective frequency-reconfigurable antenna for cognitive radio applications *IEEE Antennas Wireless Propag. Lett.*, **13** 515–518

[11] Jilani S F and Alomainy A 2017 An inkjet-printed MMW frequency-reconfigurable antenna on a flexible PET substrate for 5G wireless systems *Loughborough Antennas Propag. Conf. (LAPC)* 1–3.

[12] Jilani S F *et al* 2016 Flexible millimetre-wave frequency reconfigurable antenna for wearable applications in 5G networks *URSI Int. Symp. Electromag. Theory (EMTS)* 846–848.

[13] Romputtal A and Phongcharoenpanich C 2017 Frequency reconfigurable multiband antenna with embedded biasing network *IET Microw. Antennas Propag.* **11** 10, 1369–1378

[14] Yang X-L *et al* 2015 Frequency reconfigurable antenna for wireless communications using GaAs FET switch *IEEE Antennas Wireless Propag. Lett.* **14** 807–810

[15] Rajagopalan H *et al* 2014 MEMS reconfigurable optimized E-shaped patch antenna design for cognitive radio *IEEE Trans. Antennas Propag.* **62** 3 1056–1064

[16] Horestani A K *et al* 2016 Reconfigurable and tunable S-shaped split-ring resonators and application in band-notched UWB antennas *IEEE Trans. Antennas Propag.* **64** 9 3766–3776

[17] Prather D W *et al* 2017 Optically upconverted, spatially coherent phased-array-antenna feed networks for beam-space MIMO in 5G cellular communications *IEEE Trans. Antennas Propag.* **65**, 12 6432–6443

[18] Hussain R and Sharawi M 2016 Planar meandered-F-shaped 4-element reconfigurable multiple-input–multiple-output antenna system with isolation enhancement for cognitive radio platforms *IET Microw. Antennas Propag.* **10** 1 45–52

[19] Tehrani B *et al* 2016 Inkjet printing of multilayer millimeter-wave Yagi-Uda antennas on flexible substrates *IEEE Antennas Wireless Propag. Lett.* **15** 143–146

[20] Saeed S M *et al*. 2016 Inkjet-printed flexible reconfigurable antenna for conformal WLAN/WiMAX wireless devices *IEEE Antennas Wireless Propag. Lett.* **15** 1979–1982

[21] Xiaotian Li *et al* 2018 Flexible circuits and materials for large-area UHF RFID reader antenna systems *Flex. Print. Electron.* **3** 015005

[22] Kreit E *et al* 2017 Printed multilayer conformal x-band antenna array *Flex. Print. Electron.* **2** 045009

Accepted Manuscript

[23] Khaleel H R 2014 Design and fabrication of compact inkjet printed antennas for integration within flexible and wearable electronics *IEEE Trans. Compon. Packag*. **4** 10 1722–1728

[24] Guo X *et al* 2017 Flexible and deformable monopole antenna based on silver nanoparticles for wearable electronics *Nanoscience Nanotech. Lett.* **9** 11 1632–1638.

[25] Guo X *et al* 2017 Flexible and wearable 2.45 GHz CPW-fed antenna using inkjet-printing of silver nanoparticles on PET substrate *Microw. Optical Tech. Lett.* **59** 1 204–208

[26] Guo X *et al* 2017 Flexible and reversibly deformable radio-frequency antenna based on stretchable SWCNTs/PANI/Lycra conductive fabric *Smart Mater. Struct.* **26** 105036

[27] Kumar A *et al* 2017 A highly deformable conducting traces for printed antennas and interconnects: silver/fluoropolymer composite amalgamated by triethanolamine *Flex. Print. Electron.* **2** 045001

[28] Aboufoul T, Alomainy A, and Parini C 2013 Polarization reconfigurable ultrawideband antenna for cognitive radio applications *Microwave. Opt. Tech. Lett*. **55** 3 501–506

[29] Sridhar A *et al* 2009 Inkjet-printing- and electroless-plating-based fabrication of RF circuit structures on high-frequency substrates *J. Micromech. Microeng.* **19**, 085020

[30] Fang Y *et al* 2016 A bio-enabled maximally mild layer-by-layer Kapton surface modification approach for the fabrication of all-inkjet-printed flexible electronic devices *Sci. Rep*. **6**, 39909

[31] Rahimian A 2013 Design and performance of a Ku-band Rotman lens beamforming network for satellite systems *Progress In Electromag. Research M* **28** 41–55

[32] Ahn J *et al* 2017 Compact spiral element for wideband beam-steering arrays *IEEE Antennas Wireless Propag.Lett.* **16** 1994–1997

[33] Alreshaid A T *et al* 2016 A dual-element MIMO antenna system with a mm-wave antenna array *10th European Conf. Antennas Propag. (EuCAP)* 1–4

[34] Jilani S F and Alomainy A 2018 Millimetre-wave T-shaped MIMO antenna with defected ground structures for 5G cellular networks *IET Microw. Antennas Propag.* **12** 5 672–677

[35] Rehman M U *et al* 2017 A low profile antenna for millimeter-wave body-centric applications *IEEE Trans. Antennas Propag.* **65** 12 6329–6337

[36] Lee C, Khattak M K, and Kahng S 2018 Wideband 5G beamforming printed array clutched by LTE-A 4 × 4-multiple-input–multiple-output antennas with high isolation *IET Microw. Antennas Propag.* **12** 8 1407–1413

Accepted Manuscript